

L2COcc: Lightweight Camera-Centric Semantic Scene Completion via Distillation of LiDAR Model

Ruoyu Wang¹, Yukai Ma¹, Yi Yao¹, Sheng Tao¹, Haoang Li², Zongzhi Zhu³, Yong Liu^{1,*}, Xingxing Zuo^{2,*}

Abstract—Semantic Scene Completion (SSC) constitutes a pivotal element in autonomous driving perception systems, tasked with inferring the 3D semantic occupancy of a scene from sensory data. To improve accuracy, prior research has implemented various computationally demanding and memory-intensive 3D operations, imposing significant computational requirements on the platform during training and testing. This paper proposes L2COcc, a lightweight camera-centric SSC framework that also accommodates LiDAR inputs. With our proposed efficient voxel transformer (EVT) and cross-modal knowledge modules, including feature similarity distillation (FSD), TPV distillation (TPVD) and prediction alignment distillation (PAD), our method substantially reduce computational burden while maintaining high accuracy. The experimental evaluations demonstrate that our proposed method surpasses the current state-of-the-art vision-based SSC methods regarding accuracy on both the SemanticKITTI and SSCBench-KITTI-360 benchmarks, respectively. Additionally, our method is more lightweight, exhibiting a reduction in both memory consumption and inference time by over 23% compared to the current state-of-the-arts method. Code is available at our project page: <https://studyingfufu.github.io/L2COcc/>.

I. INTRODUCTION

Semantic Scene completion (SSC) inferring the semantic occupancy from sensor observations plays a pivotal role in autonomous driving, facilitating obstacle avoidance, path planning, and decision making. Following the seminal work by SSCNet [1], which provided a clear delineation of this task, numerous LiDAR-based methods [2–5] have been introduced, leveraging the inherent advantage of LiDAR sensors in capturing accurate geometry information of the scene. However, due to the high cost and installation limitations associated with LiDAR, researchers have shifted their focus toward visual SSC [6–9]. Likewise, this paper also emphasizes camera-centric SSC.

A critical step in visual SSC is transforming features from 2D images to 3D space. Lift, Splat, and Shoot (LSS) [10] and Deformable Cross Attention (DCA) [11, 12] represent two foundational techniques for feature transformation to generate voxel features. However, DCA-based methods face limitations due to the numerous parameters associated with

¹The authors are with the Institute of Cyber-Systems and Control, Zhejiang University, Hangzhou, China.

²The authors are with the School of Computation, Information and Technology, Technical University of Munich, Munich, Germany.

³The author is with Zhejiang Guoli Security Technology Co., Ltd., Ningbo, China.

Yong Liu is with the State Key Laboratory of Industrial Control Technology.

* Xingxing Zuo and Yong Liu are the corresponding authors (Email: xingxing.zuo@tum.de; yongliu@iipc.zju.edu.cn).

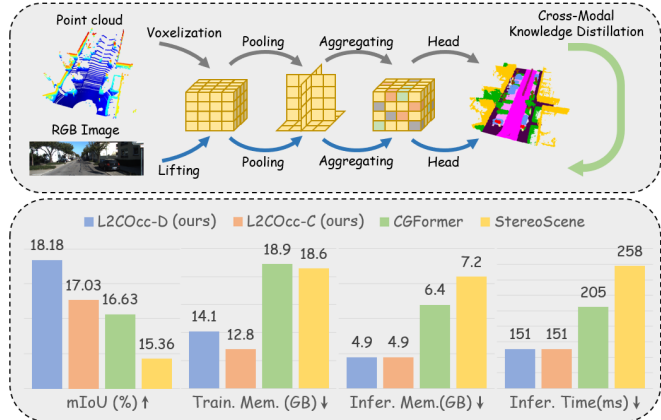


Fig. 1: Top: An overview of our framework. Bottom: Performance of our approach on SemanticKITTI [16] dataset. Our proposed L2COcc is a TPV-based lightweight camera-centric SSC framework. L2COcc-C is trained using only camera data, whereas L2COcc-D is distilled from our LiDAR model but operates solely on camera input during inference. Our approach demonstrates superior performance in terms of accuracy, memory consumption, and efficiency compared to representative methods, CGFormer [14] and StereoScene [17].

learnable voxel queries and the substantial memory consumption resulting from three-dimensional deformable self-attention (3D-DSA). Consequently, there is a pressing need for an efficient converter to transform 2D features into 3D voxel features.

Moreover, directly predicting semantic occupancy from voxel features produced by the view transformation module can lead to unsatisfying accuracy. Additional refinement steps are required for optimal performance, including the integration of an additional 3D convolutional network [13, 14], as well as multiple stages of DCA and 3D-DSA operations [7, 15]. However, these supplementary steps can lead to considerable computational and memory overhead, thereby hindering the efficiency and broad applicability of visual SSC.

Building on the identified challenges above, we propose further advancing visual SSC in this paper by reducing GPU memory usage and improving computational efficiency without compromising accuracy. Specifically, we conduct a TPV-based occupancy prediction network (see Fig. 1) that infers semantic occupancy without acquiring complex operations on 3D voxel features. Additionally, we incorporate LiDAR point cloud into the training phase, facilitating knowledge distillation to a camera-only pipeline for enhanced performance at the inference stage.

The primary contributions of this work can be summarized

as follows:

- We introduce L2COcc, a lightweight, TPV-based camera-centric framework for SSC that also accommodates LiDAR input. An efficient voxel transformer (EVT) is proposed, which significantly reduces both the number of parameters and GPU memory usage.
- We incorporate three types of cross-modal knowledge distillation modules (FSD, TPVD, PAD) applicable to the framework above, utilizing a LiDAR-based teacher to enhance the performance of a camera-based student.
- Experimental results show that our L2COcc outperforms all of the existing visual approaches on both the KITTI360 [18] and SemanticKITTI [16] benchmarks regarding Intersection over Union (IoU) and mean Intersection over Union (mIoU), despite our method having a significant reduction over 23% in both memory consumption and inference time compared to the current state-of-the-arts method.

II. RELATED WORK

A. SSC from LiDAR

SSC aims to infer semantic occupancy from sensor observation, as defined by SSCNet [1]. LiDAR sensors, due to their advantage in accurate 3D geometry measurement, have been extensively used in SSC tasks. SSCNet [1] employs 3D U-Net to voxels and suffers from high computation cost. In contrast, LMSCNet [19] adopts lighter 2D convolutions, whereas PASCO [2] employs a transformer-based sparse 3D U-Net to process 3D voxel grid. S3CNet [3] and SSC-RS [20] integrate BEV representation with voxel representation to aggregate global information. PointOcc [5] entirely replaces voxel representation with cylinder representation, resulting in a significantly more lightweight and efficient network.

B. SSC from Camera

The camera is a popular sensor for perception due to its rich semantic information and low economic cost. Pioneering work such as Monoscene [6] has positioned monocular visual SSC as a new point of interest. A key step in monocular visual SSC involves generating 3D descriptions from 2D observation. Some methods use DCA-based [11] approaches to aggregate features from images. TPVFormer [21] aggregates TPV features from images as an alternative to BEV. Voxformer [8] and Symphonize [15] enhance BEV queries by proposing depth-based and instance queries, respectively. Differently, several methods [9, 13, 14, 22] use LSS view transformer approaches to lift 2D feature to 3D voxels. CGFormer [14] fused LSS volume into voxel queries and extended the DCA operation from 2D to 3D pixel space, improving the performance of feature lifting. Our L2COcc utilizes an efficient voxel transformer (EVT) module to extract voxel features, followed by a lightweight TPV-based pipeline to infer semantic occupancy. As shown in Figure 1, L2COcc is more lightweight and efficient than compared methods, while still maintaining high accuracy.

C. Knowledge Distillation

Knowledge distillation initially focused on the transfer of knowledge between models of different specifications in image classification tasks [23], to enable smaller models to achieve high accuracy. Recent research has shown that knowledge distillation is a general technique that can be applied to a variety of tasks, including BEV object detection [24], 3D object detection [25, 26], and also semantic scene completion [4, 7, 27].

SCPNet [4] and MonoOcc [7] are LiDAR- and camera-based methods respectively that both utilize multi-frame teachers to improve the performance of single-frame students. LiCROcc [27] proposes a cross-modal distillation method for multi-sensor fusion, which transfers knowledge from the LiDAR-camera fusion model to the radar-camera fusion model, further improving radar-centric semantic occupancy prediction.

III. METHODOLOGY

Our objective is to efficiently predict the semantic occupancy of a scene from a single-frame monocular image with a lightweight model. Figure 2 shows an overview of our approach. Firstly, we leverage feature extractors to extract 3D voxel features (Section III-A) for images and LiDAR point clouds, respectively. Then, the voxel features are converted into TPV features, and processed by a TPV-based semantic occupancy prediction pipeline (Section III-B). Finally, we transfer knowledge from the LiDAR-based teacher to the camera-based student through knowledge distillation (Section III-C), further improving the performance of the camera-only model at inference.

A. Efficient Voxel Feature Extraction

Camera Branch. Given an image $\mathbf{I} \in \mathbb{R}^{H \times W \times 3}$, we initially extract 2D image feature map $\mathbf{F}_I^{2D} \in \mathbb{R}^{H \times W \times C}$ using an image encoder, EfficientNet [28]. Subsequently, we transfer the feature \mathbf{F}_I^{2D} to 3D voxel features \mathbf{F}_I^{3D} through the following two steps.

1) *LSS View Transformation*: We follow the standard LSS view transformation [10, 14] from 2D into 3D. Starting from the 2D features \mathbf{F}_I^{2D} and the predicted depth $\mathbf{Z}_I \in \mathbb{R}^{H \times W}$ from off-the-self depth prediction model [29, 30], we utilize the Depth Net and Context Net modules proposed in CGFormer [14] to generate a discrete depth probability map $\mathbf{D} \in \mathbb{R}^{H \times W \times D}$ and context feature $\mathbf{C} \in \mathbb{R}^{H \times W \times C}$, respectively. Subsequently, the outer product of \mathbf{D} and \mathbf{C} is computed to obtain the LSS feature volume, formulated as $\mathbf{F}_I^{LSS} = \mathbf{D} \otimes \mathbf{C}$. We supervise the estimated depth probability from the Depth Net by computing the loss \mathcal{L}_d [12] with the ground truth provided by LiDAR scans.

2) *Efficient Voxel Transformer (EVT)*: We back-project the depth map into a point cloud to determine each voxel's occupancy. The occupancy is represented by $\mathbf{M} \in \mathbb{R}^{X \times Y \times Z}$, where voxels occupied by points will be assigned ones otherwise zeros. The LSS feature volume is further selectively

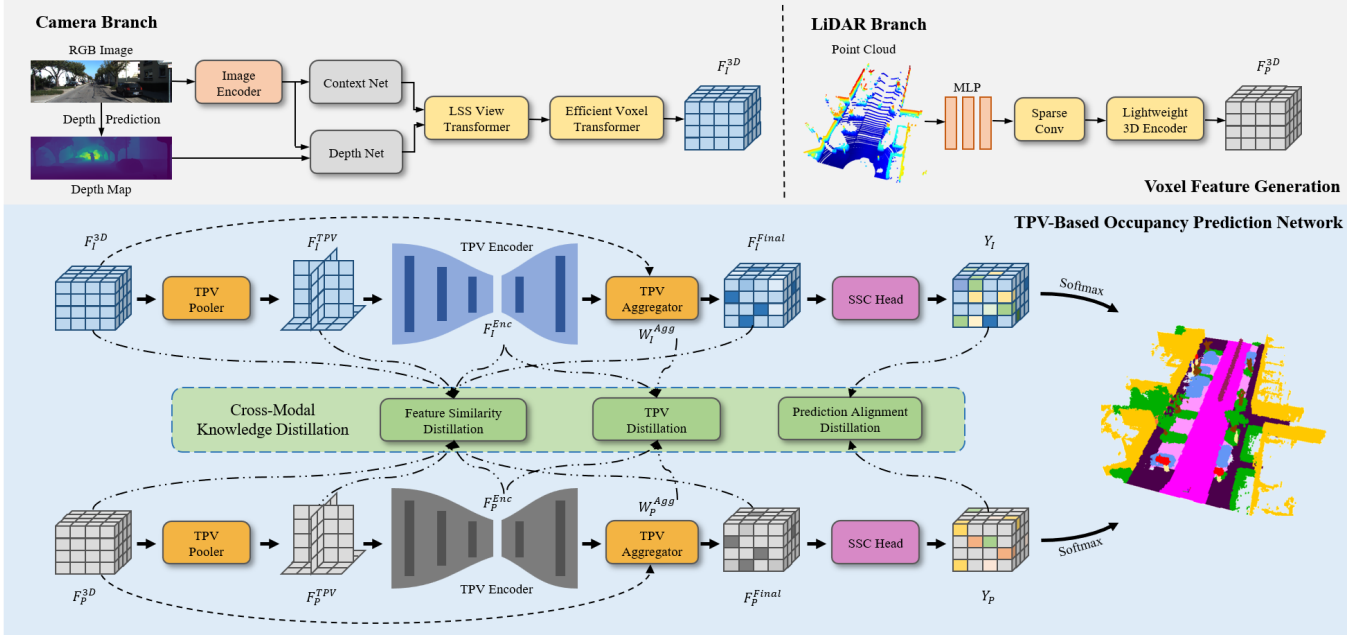


Fig. 2: The overall framework of our proposed L2COcc, comprised of three stages: voxel feature generation (indicated by the gray background), TPV-based occupancy prediction network (indicated by the blue background), and cross-modal knowledge distillation (indicated by the green background). The voxel features generated by the camera and LiDAR branches serve as inputs to the TPV-based occupancy prediction network. Meanwhile, cross-modal knowledge distillation transfers knowledge from the LiDAR-based teacher to the camera-only model during inference.

processed by 3D deformable cross-attention to obtain \mathbf{F}_I^{EVT} :

$$\mathbf{F}_I^{EVT} = \begin{cases} \text{3D-DCA}(\mathbf{F}_I^{LSS}(\mathbf{p}), \mathbf{F}_I^{LSS}, \mathbf{p}), & \text{if } M(\mathbf{p}) = 1 \\ \text{MLP}(\mathbf{F}_I^{LSS}(\mathbf{p})), & \text{if } M(\mathbf{p}) = 0 \end{cases} \quad (1)$$

In the above equations, DCA with LSS volume will be employed to aggregate high-level features if the voxel at position \mathbf{p} is occupied. Otherwise, a lightweight MLP is used to efficiently generate features. In the DCA operation, we directly utilize the LSS volume feature as the voxel query rather than using a predefined voxel embedding as existing methods [7, 8, 14, 15]. Sequentially, we employ a lightweight 3D ResNet and FPN (feature pyramid network) to further refine \mathbf{F}_I^{EVT} and get the final voxel feature \mathbf{F}_I^{3D} .

LiDAR Branch. Given a LiDAR point cloud $\mathbf{P} \in \mathbb{R}^{N \times 3}$, we follow a standard way [5] to get encoded features $\mathbf{F}_P \in \mathbb{R}^{N \times C}$, by employing a point-wise MLP and sparse convolution. We then structuralize and densify the encoded sparse features into voxel representation. Same as the camera branch, we also utilize the lightweight 3D ResNet and FPN to obtain LiDAR voxel feature \mathbf{F}_P^{3D} .

B. TPV-Based Lightweight Occupancy Prediction Network

We propose a lightweight TPV-based network to predict semantic occupancy from the 3D voxel feature \mathbf{F}^{3D} . $\mathbf{F}^{3D} = \mathbf{F}_I^{3D}$ or \mathbf{F}_P^{3D} . Our network mainly consists of four modules: (1) TPV pooler to compress the 3D voxel feature \mathbf{F}^{3D} to TPV features, (2) TPV encoder to refine TPV features, (3) TPV aggregator to integrate TPV features back to the voxel feature, and (4) SSC head to infer the semantic occupancy.

TPV Pooler. Maxpooling-based pooler is straightforward for compression, however, it inevitably incurs information loss. For effective compression, we propose a weighted average pooling operation (WAP). From the voxel features \mathbf{F}^{3D} , we compute a weight tensor $\mathbf{W} \in \mathbb{R}^{X \times Y \times Z \times 3}$ using a convolution layer ended with softmax operation. Denote the target dimension to be compressed as $d \in \{0, 1, 2\}$, WAP is formulated as:

$$\text{WAP}(\mathbf{F}, \mathbf{W}, d) = \text{SUM}((\mathbf{W}[:, :, :, d]) \odot \mathbf{F}^{3D}, d). \quad (2)$$

The function $\text{SUM}(\mathbf{F}, d)$ denotes the operation of summing the tensor \mathbf{F} along dimension d . We apply pooling operation on three dimensions to obtain three 2D feature maps $\mathbf{F}_{xy} \in \mathbb{R}^{X \times Y \times C}$, $\mathbf{F}_{yz} \in \mathbb{R}^{Y \times Z \times C}$ and $\mathbf{F}_{zx} \in \mathbb{R}^{X \times Z \times C}$.

TPV Encoder. To refine the compressed TPV features, we follow CGfomer [14] and employ a SwinTranformer-based 2D backbone [31] to extract multi-level features and use a 2D convolutional network to fuse them. We denote the processed TPV features as $\mathbf{F}^{Enc} = \{\hat{\mathbf{F}}_{xy}, \hat{\mathbf{F}}_{yz}, \hat{\mathbf{F}}_{zx}\}$.

TPV Aggregator. TPV features are initially broadcast onto the 3D space while preserving the same shape as the 3D voxel features \mathbf{F}^{3D} to facilitate aggregation operations. For example, $\hat{\mathbf{F}}_{xy} \in \mathbb{R}^{X \times Y \times C}$ is broadcast on the z dimension to get $\hat{\mathbf{F}}_{xy}^{3D} \in \mathbb{R}^{X \times Y \times Z \times C}$. The broadcast features are denoted as $\hat{\mathbf{F}}^{TPV} = \{\hat{\mathbf{F}}_{xy}^{3D}, \hat{\mathbf{F}}_{yz}^{3D}, \hat{\mathbf{F}}_{zx}^{3D}\}$. We fuse \mathbf{F}^{3D} and $\hat{\mathbf{F}}^{TPV}$ by directly summing them and then apply a convolution layer followed by a Softmax function to generate the weight tensor $\mathbf{W}^{agg} \in \mathbb{R}^{X \times Y \times Z \times 4}$. In summary, the final voxel feature

\mathbf{F}^{final} is computed as:

$$\mathbf{W}^{Agg} = \text{Softmax}(\text{Conv}(\mathbf{F}^{3D} + \sum \hat{\mathbf{F}}^{TPV})), \quad (3)$$

$$\mathbf{F}^{final} = \sum_i^4 \mathbf{W}_i^{Agg} \odot \mathbf{F}_i^{3D}. \quad (4)$$

SSC Head: We use an SSC head consisting of linear projection layers and softmax to predict the final semantic occupancy $\mathbf{Y} \in \mathbb{R}^{X \times Y \times Z \times N_c}$, where N_c denotes the number of target classes. Following [6], we train our network by minimizing the sum of three types of losses, including \mathcal{L}_{ce} , \mathcal{L}_{scal}^{geo} and \mathcal{L}_{scal}^{sem} . The three losses represent cross-entropy loss weighted by class frequencies, and scene-class affinity loss for geometry and semantics respectively.

C. Cross-Modal Knowledge Distillation

We incorporate three types of distillation at different levels, including feature similarity distillation (FSD), TPV distillation (TPVD) and prediction alignment distillation (PAD), while FSD and TPVD focus on feature-level distillation and PAD focus on prediction-level distillation.

Feature Similarity Distillation (FSD). Utilizing the same occupancy prediction network for both the camera and LiDAR modalities enables feature similarity distillation. The primary objective is to develop a loss function that minimizes the discrepancies between feature maps at corresponding levels across different modalities. As illustrated in Figure 2, we incorporate as many features as possible into the distillation process to achieve optimized outcomes. Considering the differences between the voxel feature extractors of the camera and LiDAR branches, we select cosine similarity loss as the loss function, as it exclusively focuses on the angular relationship between features while disregarding their magnitudes.

Let us denote the 2D and 3D features to distill by $\mathbf{F}_{distill}^{2D} = \{\mathbf{f}_i^{2D} \in \mathbb{R}^{h \times w \times C} | i = 0, \dots, N_{2d}\}$ and $\mathbf{F}_{distill}^{3D} = \{\mathbf{f}_i^{3D} \in \mathbb{R}^{X \times Y \times Z \times C} | i = 0, \dots, N_{3d}\}$, respectively. N_{2d} and N_{3d} represent the number of 2D and 3D feature to be distilled. To streamline the representation, we combine $\mathbf{F}_{distill}^{2D}$ and $\mathbf{F}_{distill}^{3D}$ into a single set denoted as $\mathbf{F}_{distill} = \{\mathbf{f}_i \in \mathbb{R}^{M \times C} | i = 0, \dots, N = N_{2d} + N_{3d}\}$ where M generally refers to the number of elements in the 2D or 3D feature. Furthermore, assuming that $\mathbf{f}_{i,T}(j)$ and $\mathbf{f}_{i,S}(j)$ are the j -th element of the i -th feature map from the teacher and student network, respectively. The feature similarity loss is formulated as follows:

$$\mathcal{L}_{fsd} = 1 - \frac{1}{N} \sum_{i=1}^N \frac{1}{M} \sum_{j=1}^M \frac{\mathbf{f}_{i,S}^\top(j) \mathbf{f}_{i,T}(j)}{\|\mathbf{f}_{i,S}(j)\|_2 \|\mathbf{f}_{i,T}(j)\|_2}. \quad (5)$$

TPV Distillation (TPVD): We have both the feature relation and aggregator distillation at the TPV feature level.

1) **TPV Relation Distillation (TRD):** Inspired by [27], we introduce TPV relation distillation, emphasizing the consistency of the relations among TPV features from both the teacher and student models. For instance, considering the XY plane, teacher feature $\hat{\mathbf{F}}_{xy,t}$ and student feature $\hat{\mathbf{F}}_{xy,s} \in$

$\mathbb{R}^{X \times Y \times C}$ are initially generated from the TPV encoder, we subsequently adjust the dimension of these tensors to fit within the space of $\mathbb{R}^{C \times (X \times Y)}$ and compute affinity matrix as follows:

$$C(u, v) = \frac{\mathbf{f}_u^\top \mathbf{f}_v}{\|\mathbf{f}_u\|_2 \|\mathbf{f}_v\|_2}, (u, v \in \{1, 2, \dots, K = X \times Y\}), \quad (6)$$

where $C(u, v)$ denotes the cosine similarity at each element (u, v) of the affinity matrix, \mathbf{f}_u denotes the u -th feature in the feature map \mathbf{F}_{xy} . The TRD loss on the XY plane is then defined as follows:

$$\mathcal{L}_{trd}^{xy} = \frac{1}{K \times K} \sum_{u=1}^K \sum_{v=1}^K \|\mathbf{C}_S^{xy}(u, v) - \mathbf{C}_T^{xy}(u, v)\|_1, \quad (7)$$

where \mathbf{C}_S^{xy} and \mathbf{C}_T^{xy} denote the affinity matrix of the student and teacher network's XY plane TPV feature maps, respectively, while \mathcal{L}_{trd}^{xy} quantifies the discrepancy between these matrices. The final TRD loss is computed as the sum of the contributions from three planes:

$$\mathcal{L}_{trd} = \mathcal{L}_{trd}^{xy} + \mathcal{L}_{trd}^{yz} + \mathcal{L}_{trd}^{zx} \quad (8)$$

2) **TPV Aggregator Distillation (TAD):** TPV aggregator distillation directly aligns the student's weight distribution with the teacher's, thereby facilitating the student's convergence towards the teacher's parameters. Inspired by Monoscene [6], we employ KL Divergence [36] loss to measure the difference in aggregating weight distribution, assuming that \mathbf{W}_S^{Agg} and \mathbf{W}_T^{Agg} , calculated by Equation 3, represent the weight tensors from the student and teacher models, respectively, TPV aggregator distillation loss, denoted as \mathcal{L}_{tad} is computed as follows:

$$\mathcal{L}_{tad} = \text{KL}(\mathbf{W}_S^{Agg} || \mathbf{W}_T^{Agg}) \quad (9)$$

Prediction Alignment Distillation (PAD): Prediction alignment distillation seeks to align the student and teacher models by minimizing the distributional discrepancies. Like TPV aggregator distillation, we also use KL Divergence loss to measure the difference in distribution between predicted targets. The PAD loss is computed as follows:

$$\mathcal{L}_{pad} = \text{KL}(\tilde{\mathbf{Y}}_S || \tilde{\mathbf{Y}}_T) \quad (10)$$

D. Training Loss

In this section, we will review all the loss functions previously mentioned and summarize them into an overall loss function. To optimize the Depth Net in the view transformer, we incorporate \mathcal{L}_d (Section III-A). For occupancy prediction network, we employ \mathcal{L}_{ce} , \mathcal{L}_{scal}^{geo} , \mathcal{L}_{scal}^{sem} (Section III-B). To enable the knowledge distillation, we take \mathcal{L}_{fsd} , \mathcal{L}_{trd} , \mathcal{L}_{tad} and \mathcal{L}_{pad} into use (Section III-C). The overall loss function is formulated as follows:

$$\mathcal{L} = \lambda_1 \mathcal{L}_{ce} + \lambda_2 \mathcal{L}_{scal}^{geo} + \lambda_3 \mathcal{L}_{scal}^{sem} + \lambda_4 \mathcal{L}_d + \lambda_5 \mathcal{L}_{fsd} + \lambda_6 \mathcal{L}_{trd} + \lambda_7 \mathcal{L}_{tad} + \lambda_8 \mathcal{L}_{pad} \quad (11)$$

TABLE I: Performance on SemanticKITTI[16] (test set). The C, L denotes input modality of camera and LiDAR, respectively. We mark the best and the second best score in **bold** and underlined and mark \dagger after the temporal stereo-based methods.

Method	Input	IoU	mIoU																					
				road	sidewalk	parking	other-grnd.	building	car	truck	bicycle	motorcycle	other-veh.	vegetation	trunk	terrain	person	bicyclist	motorcyclist	fence	pole	traffic-sign		
MonoScene [6]	C	34.16	11.08	54.70	27.10	24.80	5.70	14.40	18.80	3.30	0.50	0.70	4.40	14.90	2.40	19.50	1.00	1.40	0.40	11.10	3.30	2.10		
TPVFormer [21]	C	34.25	11.26	55.10	27.20	27.40	6.50	14.80	19.20	3.70	1.00	0.50	2.30	13.90	2.60	20.40	1.10	2.40	0.30	11.00	2.90	1.50		
OccFormer [13]	C	34.53	12.32	55.90	30.30	31.50	6.50	15.70	21.60	1.20	1.50	1.70	3.20	16.80	3.90	21.30	2.20	1.10	0.20	11.90	3.80	3.70		
IAMSSC [32]	C	43.74	12.37	54.00	25.50	24.70	6.90	19.20	21.30	3.80	1.10	0.60	3.90	22.70	5.80	19.40	1.50	2.90	0.50	11.90	5.30	4.10		
DepthSSC [33]	C	<u>44.58</u>	13.11	55.64	27.25	25.72	5.78	20.46	21.94	3.74	1.35	0.98	4.17	23.37	7.64	21.56	1.34	2.79	0.28	12.94	5.87	6.23		
VoxFormer-T \dagger [8]	C	43.21	13.41	54.10	26.90	25.10	7.30	23.50	21.70	3.60	1.90	1.60	4.10	24.40	8.10	24.20	1.60	1.10	0.00	13.10	6.60	5.70		
HASSC-T \dagger [34]	C	42.87	14.38	55.30	29.60	25.90	11.30	23.10	23.00	2.90	1.90	1.50	4.90	24.80	9.80	26.50	1.40	3.00	0.00	14.30	7.00	7.10		
H2GFormer-T \dagger [35]	C	43.52	14.60	57.90	30.40	30.00	6.90	24.00	23.70	<u>5.20</u>	0.60	1.20	5.00	25.20	10.70	25.80	1.10	0.10	0.00	14.60	7.50	<u>9.30</u>		
Symphonize [15]	C	42.19	15.04	58.40	29.30	26.90	11.70	24.70	23.60	3.20	3.60	2.60	5.60	24.20	10.00	23.10	3.20	1.90	2.00	16.10	7.70	8.00		
StereoScene [17]	C	43.34	15.36	61.90	31.20	30.70	10.70	24.20	22.80	2.80	3.40	2.40	6.10	23.80	8.40	27.00	<u>2.90</u>	2.20	0.50	16.50	7.00	7.20		
MonoOcc-S [7]	C	-	13.80	55.20	27.80	25.10	9.70	21.40	23.20	<u>5.20</u>	2.20	1.50	5.40	24.00	8.70	23.00	1.70	2.00	0.20	13.40	5.80	6.40		
MonoOcc-L [7]	C	-	15.63	59.10	30.90	27.10	9.80	22.90	23.90	7.20	<u>4.50</u>	2.40	7.70	25.00	9.80	26.10	2.80	4.70	<u>0.60</u>	16.90	7.30	8.40		
CGFormer [14]	C	44.41	16.63	64.30	34.20	<u>34.10</u>	12.10	25.80	26.10	4.30	3.70	1.30	2.70	24.50	11.20	29.30	1.70	<u>3.60</u>	0.40	18.70	8.70	<u>9.30</u>		
L2COcc-C (Ours)	C	44.31	17.03	66.00	35.00	33.10	13.50	25.10	27.20	3.00	3.50	3.60	4.30	25.20	<u>11.50</u>	30.10	1.50	2.40	0.20	<u>20.50</u>	9.10	8.90		
L2COcc-D (Ours)	C	45.37	18.18	68.20	36.90	34.60	16.20	25.80	28.30	4.50	4.90	<u>3.30</u>	7.20	26.20	11.90	32.00	2.10	2.40	0.30	21.60	9.60	9.50		
L2COcc-L (Ours)	L	60.32	23.37	68.50	40.60	33.20	6.10	41.50	36.80	5.40	8.70	4.10	9.00	42.60	28.70	36.90	1.40	2.90	1.00	27.70	27.00	21.90		

TABLE II: Performance on SSCBench-KITTI360[18] (test set). We also mark the best and the second best score in **bold** and underlined.

Method	Input	IoU	mIoU																					
				car	bicycle	motorcycle	truck	other-veh.	person	road	parking	sidewalk	other-grnd.	building	fence	vegetation	terrain	pole	traffic-sign	other-struct.	other-obj.			
MonoScene [6]	C	37.87	12.31	19.34	0.43	0.58	8.02	2.03	0.86	48.35	11.38	28.13	3.32	32.89	3.53	26.15	16.75	6.92	5.67	4.20	3.09			
TPVFormer [21]	C	40.22	13.64	21.56	1.09	1.37	8.06	2.57	2.38	52.99	11.99	31.07	3.78	34.83	4.80	30.08	17.52	7.46	5.86	5.48	2.70			
OccFormer [13]	C	40.27	13.81	22.58	0.66	0.29	9.89	3.82	2.77	54.30	13.44	31.53	3.55	36.42	4.80	31.00	19.51	7.77	8.51	6.95	4.60			
VoxFormer [8]	C	38.76	11.91	17.84	1.16	0.89	4.56	2.06	1.63	47.01	9.67	27.21	2.89	31.18	4.97	28.99	14.69	6.51	6.92	3.79	2.43			
IAMSSC [32]	C	41.80	12.97	18.53	2.45	1.76	5.12	3.92	3.09	47.55	10.56	28.35	4.12	31.53	6.28	29.17	15.24	8.29	7.01	6.35	4.19			
DepthSSC [33]	C	40.85	14.28	21.90	2.36	4.30	11.51	4.56	2.92	50.88	12.89	30.27	2.49	37.33	5.22	29.61	21.59	5.97	7.71	5.24	3.51			
Symphonies [15]	C	44.12	18.58	<u>30.02</u>	1.85	5.90	25.07	12.06	8.20	54.94	13.83	32.76	6.93	35.11	<u>8.58</u>	38.33	11.52	14.01	9.57	14.44	11.28			
CGFormer [14]	C	<u>48.07</u>	20.05	29.85	3.42	3.96	<u>17.59</u>	6.79	6.63	<u>63.85</u>	17.15	<u>40.72</u>	5.53	42.73	8.22	38.80	<u>24.94</u>	<u>16.24</u>	17.45	10.18	6.77			
L2COcc-C (Ours)	C	48.07	20.11	29.62	3.71	4.35	14.93	8.35	7.23	63.31	17.91	40.51	5.23	<u>42.78</u>	8.52	39.35	24.52	16.22	18.44	10.24	6.79			
L2COcc-D (Ours)	C	48.83	20.99	30.57	<u>3.70</u>	<u>4.63</u>	17.34	<u>9.73</u>	7.00	64.19	18.35	41.24	<u>6.42</u>	43.91	9.72	39.88	26.02	16.26	19.40	<u>10.65</u>	<u>8.87</u>			
L2COcc-L (Ours)	L	57.60	25.22	40.41	4.08	4.23	26.15	10.30	9.94	70.01	22.62	46.16	8.78	51.04	14.34	47.60	31.33	24.89	21.64	13.96	6.41			

where λ_1 to λ_8 are hyper-parameters. We set the values of these hyper parameters to be 3, 1.5, 0.5, 0.001, 4, 5, 10, 70, respectively, in our experiments.

IV. EXPERIMENTS

A. Datasets And Metrics

We evaluate our algorithm on the SemanticKITTI [16] and SSCBench-KITTI360 datasets [18]. Both datasets provide heterogeneous sensor measurements, including stereo RGB images and LiDAR scans. Dense semantic occupancy annotations are available for 22 and 9 urban driving sequences, respectively, covering the range of $51.2m \times 51.2m \times 6.4m$, represented as voxel grids of $256 \times 256 \times 32$, with a voxel size of 0.2 m. We report the commonly-used metrics for SSC tasks, including mIoU and IoU regarding the accuracy, along with memory usage and inference time for efficiency.

TABLE III: Memory usage and inference time tested on the SemanticKITTI dataset. In alignment with [14], these metrics are measured on the NVIDIA RTX 4090 GPU.

Method	mIoU	Train. Mem.	Infer. Mem.	Infer. Time
Symphonize [15]	15.04	17757M	6360M	216ms
StereoScene [17]	15.36	19000M	7329M	258ms
MonoOcc-S [7]	13.80	18432M	8192M	295ms
CGFormer [14]	16.63	19330M	6550M	205ms
L2COcc-C (Ours)	17.03	13068M	5012M	151ms
L2COcc-D (Ours)	18.18	14528M	5012M	151ms

B. Implementation Details

We train our L2COcc for 25 epochs on NVIDIA RTX 4090 GPUs, using batch sizes of 4 and 8 for SemanticKITTI [16] and SSCBench-KITTI360 [18] benchmarks, respectively. We adopt AdamW optimizer, initialized

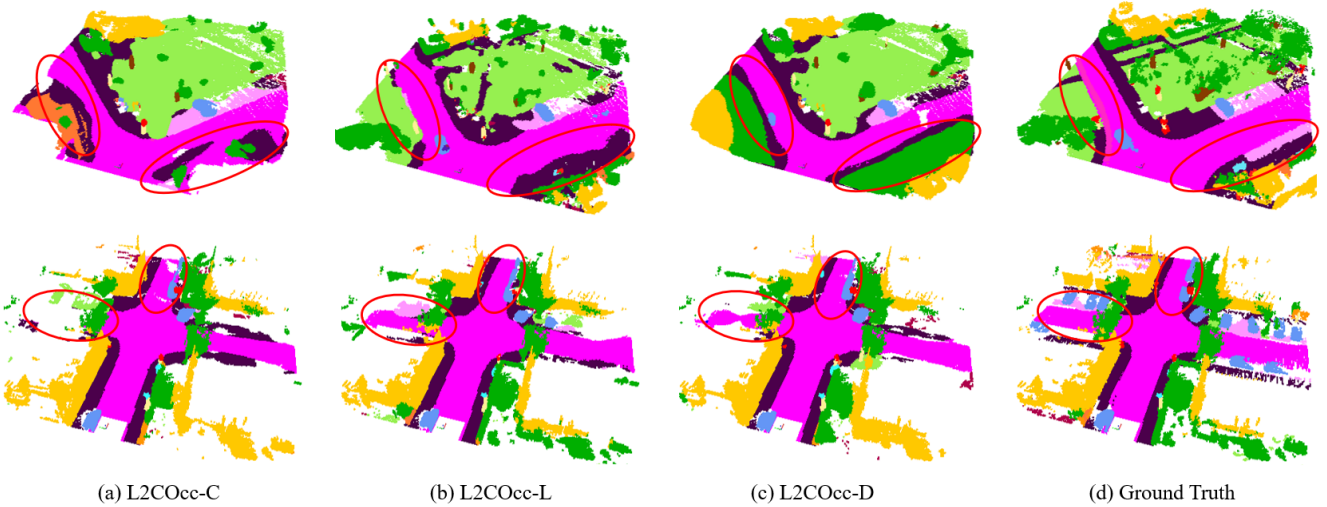


Fig. 3: Qualitative visualizations on SemanticKITTI and SSCBench-KITTI360. The introduction of cross-modal knowledge distillation enables L2COcc-D to achieve superior performance compared to L2COcc-C, particularly in regions farther from the camera and at the boundaries of the camera’s field of view.

with the maximum learning rate of 2e-4 and weight decay of 1e-2. The learning rate is adjusted according to a cosine annealing strategy.

C. Quantitative Results

We conduct comparative experiments on both SemanticKITTI and SSCBench-KITTI360 datasets. We concisely denote our camera-based model and LiDAR-based model as L2COcc-C and L2COcc-L respectively, and refer to the camera-based model employing cross-modal knowledge distillation as L2COcc-D. Table I and III present a comparison of our L2COcc and the state-of-the-art methods (SOTA) on the SemanticKITTI dataset. We only compare our L2COcc with camera-based methods, as L2COcc-C and L2COcc-D require camera input only during inference. As demonstrated in Table I, our visual-base methods L2COcc-D and L2COcc-C achieve mIoU of 18.18 and 17.03, ranking first and second in semantic prediction, respectively. Cross-modal knowledge distillation significantly enhances accuracy across nearly all categories. Table III indicates that L2COcc completes scene inference in 151 milliseconds and utilizes memory less than 5GB GPU, leading to over a 23% savings in both memory usage and inference time compared to the second-best method. Simultaneously, the reduction in GPU memory usage during training enables L2COcc to be trained on a more cost-effective computing platform. Moreover, we achieve SOTA performance on the SSC-KITTI360 dataset (Table II), further demonstrating the excellence of our L2COcc.

D. Ablation Studies

To validate the efficacy of our proposed module, we conduct a series of ablation experiments on the validation set of SemanticKITTI.

Ablation on Efficient Voxel Transformer (EVT). This section aims to elucidate the rationale and effectiveness

of the enhancements made to the voxel feature extraction process (see Sec. III-A). In contrast to CGFormer [14] that integrates the LSS volume with learnable voxel embeddings as voxel queries, subsequently generating voxel features through 3D-DCA and 3D-DSA modules, we directly use the LSS volume as voxel queries and replace 3D-DSA module with a lightweight 3D encoder. The findings in Table IV indicate that the 3D-DSA module consumes up to 6G of GPU memory, yet it leads to no significant performance enhancements. Additionally, the voxel embedding introduces 34 million extra parameters but maintains almost the same mIoU as the version without voxel embedding. The 4-th row of Table IV demonstrates that our lightweight 3D encoder is effective in enhancing the model’s performance.

TABLE IV: Ablation on efficient voxel transformer.

row	3D-DSA	Voxel Embedding	3D Encoder	mIoU	Parameters	Train Mem.
1	✓	✓	✗	15.86	148M	17448M
2	✗	✓	✗	16.34	148M	11326M
3	✗	✗	✗	16.40	114M	10849M
4	✗	✗	✓	16.72	119M	13068M

Ablation on TPV Processing Modules. The outcomes presented in Table V underscore the effectiveness of our proposed TPV pooler and TPV aggregator (see Sec. III-B) by comparing them with the TPV processing modules utilized in CGFormer. GMP denotes the Grouped Max Pooling and WAP denotes the Weighted Average Pooling we proposed. $\text{Agg}_{\text{CGFormer}}$ and $\text{Agg}_{\text{L2COcc}}$ denotes the operation aggregating TPV feature proposed by CGFormer and our L2COcc. It is shown that substituting GMP with WAP results in a 0.34 mIoU improvement. Furthermore, refinements to the TPV aggregator contributed to an additional 0.54 mIoU enhancement.

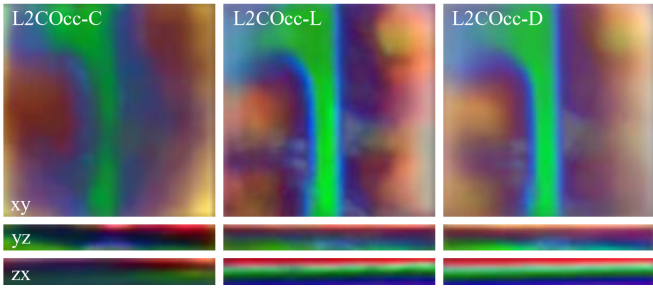


Fig. 4: PCA visualization results of TPV features F^{Enc} . F^{Enc} acquired from LiDAR exhibit a distinctive and well-defined scene geometry, whereas F^{Enc} acquired from the camera display a blurred and radial appearance. The introduction of knowledge distillation effectively addresses this challenge. More qualitative results are provided at our project page: <https://studyingfufu.github.io/L2COcc/>.

TABLE V: Ablation on TPV processing modules.

row	TPV Pooler	TPV Aggregator	mIoU
2	GMP	$Agg_{CGFormer}$	15.84
3	WAP	$Agg_{CGFormer}$	16.18
4	WAP	Agg_{L2COcc}	16.72

Ablation on Feature-Level Distillation (FSD,TPVD). FSD and TPVD aim to minimize feature discrepancies between the teacher and student models, thus referred to as feature-level distillation (see Sec. III-C). TRD and PAD exhibit a more pronounced effect only when applied in tandem, and thus, we report only the combined results. The first three rows of Table VI indicate a progressive increase in mIoU from 16.72 to 17.25 with the integration of the FSD and TPVD modules. The qualitative findings presented in Figures 4 and 5 demonstrate that the FSD and TPVD modules promote the convergence of the student model’s TPV features and TPV aggregation weights to align with those of the teacher model.

TABLE VI: Ablation on Cross-Modal Knowledge Distillation.

row	FSD	TPVD	PAD	mIoU
1	✗	✗	✗	16.72
2	✓	✗	✗	16.99
3	✓	✓	✗	17.25
4	✗	✗	✓	17.88
5	✓	✓	✓	18.22

Ablation on Prediction Alignment Distillation (PAD). The PAD module directly affects the network’s output to ensure alignment between the student network’s prediction distribution and the teacher model’s (see Sec. III-C). The penultimate and final rows of Table VI illustrate the impact of employing the PAD module independently and in tandem with FSD and TPVD. The findings reveal that the standalone use of PAD can improve the mIoU by 1.16, with enhanced performance observed when integrated with FSD and TPVD. The combined application of both techniques results in a mIoU boost of up to 1.5. The visualization results in 3 fur-

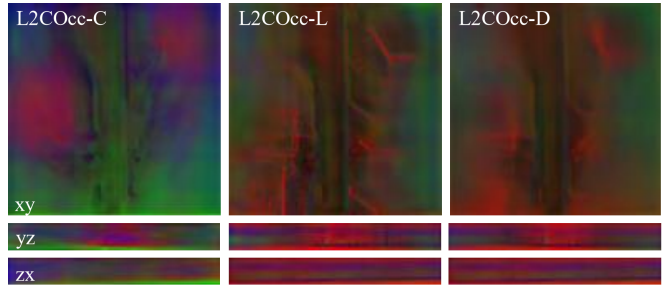


Fig. 5: Visualization results of TPV aggregating weight W^{Agg} . We compute the average of the 3D weights across each dimension to generate three corresponding 2D weight maps. Subsequently, the weights associated with the TPV features’ XY, YZ, and ZX planes are mapped to the R, G, and B channels, respectively. It’s shown that the camera-based model emphasizes the YZ plane more, whereas the LiDAR-based model assigns more weight to the XY plane. Incorporating TPV aggregator distillation enables the camera model to adopt the weight allocation pattern learned by the LiDAR model.

ther demonstrate the effectiveness of cross-modal knowledge distillation.

V. CONCLUSION

This paper introduces L2COcc, a lightweight camera-centric SSC network that also supports LiDAR input. We propose an efficient voxel transformer, and develop a TPV-based occupancy prediction pipeline for accurate and efficient SSC. Promising performance is attained by applying knowledge distillation from the LiDAR-based model to the camera-based model. Experiments show our L2COcc achieves state-of-the-art results on SemanticKITTI and SSCBench-KITTI360 while consuming significantly less memory and computation time. For future work, it is worth investigating attentive distillation from the LiDAR model to the camera model, to accommodate the performance variations of models in different scenarios.

REFERENCES

- [1] S. Song, F. Yu, A. Zeng, A. X. Chang, M. Savva, and T. Funkhouser. “Semantic scene completion from a single depth image”. In: *Proceedings of the IEEE conference on computer vision and pattern recognition*. 2017, pp. 1746–1754.
- [2] A.-Q. Cao, A. Dai, and R. de Charette. “PaSCo: Urban 3D Panoptic Scene Completion with Uncertainty Awareness”. In: (2023).
- [3] R. Cheng, C. Agia, Y. Ren, X. Li, and L. Bingbing. “S3cnet: A sparse semantic scene completion network for lidar point clouds”. In: *Conference on Robot Learning*. PMLR. 2021, pp. 2148–2161.
- [4] Z. Xia, Y. Liu, X. Li, X. Zhu, Y. Ma, Y. Li, Y. Hou, and Y. Qiao. “SCPNet: Semantic Scene Completion on Point Cloud”. In: *Proceedings of the IEEE/CVF Conference on Computer Vision and Pattern Recognition*. 2023, pp. 17642–17651.
- [5] S. Zuo, W. Zheng, Y. Huang, J. Zhou, and J. Lu. “Pointocc: Cylindrical tri-perspective view for point-based 3d semantic occupancy prediction”. In: *arXiv preprint arXiv:2308.16896* (2023).
- [6] A.-Q. Cao and R. De Charette. “Monoscene: Monocular 3d semantic scene completion”. In: *Proceedings of the IEEE/CVF Conference on Computer Vision and Pattern Recognition*. 2022, pp. 3991–4001.

[7] Y. Zheng, X. Li, P. Li, Y. Zheng, B. Jin, C. Zhong, X. Long, H. Zhao, and Q. Zhang. “Monoocc: Digging into monocular semantic occupancy prediction”. In: *arXiv preprint arXiv:2403.08766* (2024).

[8] Y. Li, Z. Yu, C. Choy, C. Xiao, J. M. Alvarez, S. Fidler, C. Feng, and A. Anandkumar. “Voxformer: Sparse voxel transformer for camera-based 3d semantic scene completion”. In: *Proceedings of the IEEE/CVF Conference on Computer Vision and Pattern Recognition*. 2023, pp. 9087–9098.

[9] J. Mei, Y. Yang, M. Wang, J. Zhu, X. Zhao, J. Ra, L. Li, and Y. Liu. “Camera-based 3d semantic scene completion with sparse guidance network”. In: *arXiv preprint arXiv:2312.05752* (2023).

[10] J. Philion and S. Fidler. “Lift, splat, shoot: Encoding images from arbitrary camera rigs by implicitly unprojecting to 3d”. In: *Computer Vision-ECCV 2020: 16th European Conference, Glasgow, UK, August 23–28, 2020, Proceedings, Part XIV 16*. Springer. 2020, pp. 194–210.

[11] X. Zhu, W. Su, L. Lu, B. Li, X. Wang, and J. Dai. “Deformable DETR: Deformable Transformers for End-to-End Object Detection”. en-US. In: *arXiv: Computer Vision and Pattern Recognition,arXiv: Computer Vision and Pattern Recognition* (2020).

[12] Z. Li, W. Wang, H. Li, E. Xie, C. Sima, T. Lu, Y. Qiao, and J. Dai. “Bevformer: Learning bird’s-eye-view representation from multi-camera images via spatiotemporal transformers”. In: *European conference on computer vision*. Springer. 2022, pp. 1–18.

[13] Y. Zhang, Z. Zhu, and D. Du. “OccFormer: Dual-path Transformer for Vision-based 3D Semantic Occupancy Prediction”. In: *arXiv preprint arXiv:2304.05316* (2023).

[14] Z. Yu, R. Zhang, J. Ying, J. Yu, X. Hu, L. Luo, S. Cao, and H. Shen. “Context and Geometry Aware Voxel Transformer for Semantic Scene Completion”. In: *arXiv preprint arXiv:2405.13675* (2024).

[15] H. Jiang, T. Cheng, N. Gao, H. Zhang, W. Liu, and X. Wang. “Symphonize 3D Semantic Scene Completion with Contextual Instance Queries”. In: *arXiv preprint arXiv:2306.15670* (2023).

[16] J. Behley, M. Garbade, A. Milioto, J. Quenzel, S. Behnke, C. Stachniss, and J. Gall. “SemanticKITTI: A dataset for semantic scene understanding of lidar sequences”. In: *Proceedings of the IEEE International Conference on Computer Vision*. 2019, pp. 9297–9307.

[17] B. Li, Y. Sun, X. Jin, W. Zeng, Z. Zhu, X. Wang, Y. Zhang, J. Okae, H. Xiao, and D. Du. “Stereoscene: Bev-assisted stereo matching empowers 3d semantic scene completion”. In: *arXiv preprint arXiv:2303.13959* 1.3 (2023), p. 6.

[18] Y. Li, S. Li, X. Liu, M. Gong, K. Li, N. Chen, Z. Wang, Z. Li, T. Jiang, F. Yu, et al. “SSCBench: A Large-Scale 3D Semantic Scene Completion Benchmark for Autonomous Driving”. In: *arXiv preprint arXiv:2306.09001* (2023).

[19] L. Roldão, R. de Charette, and A. Verroust-Blondet. “LM-SCNet: Lightweight Multiscale 3D Semantic Completion”. In: *3DV 2020-International Virtual Conference on 3D Vision*. 2020.

[20] J. Mei, Y. Yang, M. Wang, T. Huang, X. Yang, and Y. Liu. “SSC-RS: Elevate LiDAR Semantic Scene Completion with Representation Separation and BEV Fusion”. In: *2023 IEEE/RSJ International Conference on Intelligent Robots and Systems (IROS)*. IEEE. 2023, pp. 1–8.

[21] Y. Huang, W. Zheng, Y. Zhang, J. Zhou, and J. Lu. “Tri-perspective view for vision-based 3d semantic occupancy prediction”. In: *Proceedings of the IEEE/CVF Conference on Computer Vision and Pattern Recognition*. 2023, pp. 9223–9232.

[22] Z. Li, Z. Yu, D. Austin, M. Fang, S. Lan, J. Kautz, and J. M. Alvarez. “Fb-occ: 3d occupancy prediction based on forward-backward view transformation”. In: *arXiv preprint arXiv:2307.01492* (2023).

[23] G. Hinton, O. Vinyals, and J. Dean. “Distilling the Knowledge in a Neural Network”. en-US. In: *arXiv: Machine Learning,arXiv: Machine Learning* (2015).

[24] S. Zhou, W. Liu, C. Hu, S. Zhou, and C. Ma. “UniDistill: A Universal Cross-Modality Knowledge Distillation Framework for 3D Object Detection in Bird’s-Eye View”. en-US. In: (2023).

[25] Z. Wang, D. Li, C. Luo, C. Xie, and X. Yang. “DistillBEV: Boosting Multi-Camera 3D Object Detection with Cross-Modal Knowledge Distillation”. en-US. In: (2023).

[26] Y. Hong, H. Dai, and Y. Ding. “Cross-Modality Knowledge Distillation Network for Monocular 3D Object Detection”. en-US. In: () .

[27] Y. Ma, J. Mei, X. Yang, L. Wen, W. Xu, J. Zhang, B. Shi, Y. Liu, and X. Zuo. *LiCROcc: Teach Radar for Accurate Semantic Occupancy Prediction using LiDAR and Camera*. 2024. *arXiv: 2407.16197 [cs.CV]* .

[28] M. Tan. “Efficientnet: Rethinking model scaling for convolutional neural networks”. In: *arXiv preprint arXiv:1905.11946* (2019).

[29] S. F. Bhat, I. Alhashim, and P. Wonka. “Adabins: Depth estimation using adaptive bins”. In: *Proceedings of the IEEE/CVF conference on computer vision and pattern recognition*. 2021, pp. 4009–4018.

[30] F. Shamsafar, S. Woerz, R. Rahim, and A. Zell. “Mobilestereonet: Towards lightweight deep networks for stereo matching”. In: *Proceedings of the ieee/cvf winter conference on applications of computer vision*. 2022, pp. 2417–2426.

[31] Z. Liu, Y. Lin, Y. Cao, H. Hu, Y. Wei, Z. Zhang, S. Lin, and B. Guo. “Swin transformer: Hierarchical vision transformer using shifted windows”. In: *Proceedings of the IEEE/CVF international conference on computer vision*. 2021, pp. 10012–10022.

[32] H. Xiao, H. Xu, W. Kang, and Y. Li. “Instance-Aware Monocular 3D Semantic Scene Completion”. In: *IEEE Transactions on Intelligent Transportation Systems* 25.7 (2024), pp. 6543–6554.

[33] J. Yao and J. Zhang. “Depthssc: Depth-spatial alignment and dynamic voxel resolution for monocular 3d semantic scene completion”. In: *arXiv preprint arXiv:2311.17084* (2023).

[34] S. Wang, J. Yu, W. Li, W. Liu, X. Liu, J. Chen, and J. Zhu. “Not all voxels are equal: Hardness-aware semantic scene completion with self-distillation”. In: *Proceedings of the IEEE/CVF Conference on Computer Vision and Pattern Recognition*. 2024, pp. 14792–14801.

[35] Y. Wang and C. Tong. “H2gformer: Horizontal-to-global voxel transformer for 3d semantic scene completion”. In: *Proceedings of the AAAI Conference on Artificial Intelligence*. Vol. 38. 6. 2024, pp. 5722–5730.

[36] S. Kullback and R. A. Leibler. “On information and sufficiency”. In: *The annals of mathematical statistics* 22.1 (1951), pp. 79–86.